Static and dynamic testing of a full-composite VLA by using digital image correlation and output only ground vibration testing

Static and dynamic testing of a full-composite VLA by using digital image correlation and output only ground vibration testing

A. Pagani[a*], R. Azzara[a], E. Carrera[ab], E. Zappino[a]

[a]MUL2 group, Department of Mechanical and Aerospace Engineering
Politecnico di Torino, Corso Duca degli Abruzzi 24, 10129 Torino, Italy
[b]Department of mechanical engineering, college of engineering
Prince Mohammad Bin Fahd University P.O. Box 1664. Al Khobar 31952.
Kingdom of Saudi Arabia

Abstract: *This paper shows some important results from a test campaign conducted on the Dardo Aspect, a wet-laminate full-composite very-light airplane (VLA). Both static and dynamic experimental analyses are carried out. All the results and methodologies utilized in this paper take into account compliance with certification requirements. Particular attention is dedicated to demonstrating the reliability of some innovative techniques, such as the Digital Image Correlation (DIC), the operational modal analysis (OMA) and the taxing vibration test (TVT), which cannot yet be used for certification purposes. As a matter of fact, these techniques allow for a significant reduction in time and costs although may present some problems related to calibration and testing preparation.*

Keywords: Very-light airplane; Wing-up bending test; Digital image correlation; Ground vibration test; Operational modal analysis; Flutter; Taxing vibration test; Flight test.

1 Introduction

Besides the numerical analysis, experimental tests have always been a fundamental part of the development and qualification of structures of engineering interest. This is particularly true when advanced and complex materials are used, such as composites that are widely utilized nowadays for aerospace application [1]. Moreover, modern engineering design needs to manage conflicting goals:

*Corresponding author. E-mail: alfonso.pagani@polito.it

increasing performance while reducing developing time and costs. As reported by Szkudlarek *et al.* [2], to meet these challenges, the preparation of the tests plays a fundamental role. Nonetheless, in the aerospace industry, qualification testing is a standard requirement, and several static and dynamic tests shall be performed to demonstrate compliance with the certification requirements. In the open literature, there are many papers devoted to the dynamic analysis. For instance, Yan *et al.* [3] performed dynamic analyses of laser shock response providing experimental and numerical studies. Pagani *et al.* [4] dealt with the dynamic response of aerospace structures by means of refined beam theories.

This paper presents some relevant results obtained from the test campaigns conducted on the Dardo Aspect, which is a training very-light aircraft (VLA). As for the static tests, both destructive and non-destructive wing tests were performed. To do so, an innovative technique that is the Digital Image Correlation (DIC) has been used. DIC has emerged as a leading technology in structures and materials characterization [5]. As described by Pagani *et al.* [6], DIC is a non-contact, optical methodology that employs tracking and image registration techniques for accurate 2D and 3D measurements of changes in images. This method, applied in many engineering fields, is used to measure full-field, three-dimensional displacements, and in-plane strains. Regarding aerospace engineering, Vialettes *et al.* [7] used DIC to measure the strain fields over the surface of long duration superpressure balloon in realistic flight conditions. Here, we compare the results from DIC acquisitions with a Finite Element Model (FEM) of the composite wing of the Dardo, which is analyzed by using Nastran [8].

On the other hand, we discuss some relevant results from dynamic tests, which include ground vibration test (GVT), flutter clearance, taxing vibration test (TVT), and flight test. The dynamic characteristics play an important role in flutter [9] and dynamic loads. For understanding and performing aeroelastic analysis and dynamic load analysis, the primary input are the stiffness, the mass and inertia properties of each component. As a consequence, first of all, GVT analyses are carried out both on the isolated Dardo wing and the full-aircraft. GVT is one of the standard test used in the aircraft industry. As reported by Hernàndez *et al.* [10], ground vibration test is a crucial step in the design process of a new aircraft. Modern solutions for ground vibration test of large aircraft (for example, A330) are reported by Peeters *et al.* [11]. Böswald *et al.* [12] present recent advances in ground vibration test and flight vibration test. As reported by Voracek [13], in order to certify an airplane, it is essential to demonstrate its dynamic stability. GVTs determine stiffness distribution, natural frequencies, mode shapes, and damping [14]. They are necessary to

make reliable flutter predictions, to validate and update the mathematical model of the aircraft, and for the certification process. According to Gloth *et al.* [15], GVT modes are considered to be critical in the following cases: they significantly differ from the predictions, they show non-linear behaviour, or they are important for flutter calculations. Simsiriwong and Sullivan [16] stated that one of the major methods to obtain the modal characteristics of an airplane structure is by the use of Frequency-Response-Functions (FRFs). As reported by Ameri *et al.* [17], the procedures developed for the classical experimental modal analysis (EMA) typically require the structure to be installed in a laboratory, or a hangar, under conditions where simultaneous measurements of both the response and the loadings at specific points of the considered structure are possible. Nevertheless, the demand for a reduction in the overall time and cost drove the need for performing experimental tests in operating conditions. For this purpose, operational modal analysis (OMA) techniques were developed in recent years. OMA aims at identifying the modal properties of a structure based on response data of the structure excited by ambient sources. Unlike EMA, OMA makes use of operational conditions to excite the structure and is it helpful in case the excitation is inaccessible to be measured or difficult to be applied. This method is sometimes called "output-only modal analysis" because only the response of the structure is measured. The research activity around the theoretical basis of the OMA has largely increased [18], and powerful OMA techniques have been developed in both the time- and frequency-domains in order to identify the modal parameters of an aeronautical structure in operating conditions. Neu *et al.* [19] focused their studies on modal parameter extraction from a large scale wind tunnel wing model excited by transonic flow using two OMA-techniques. Furthermore, the same authors compared the OMA data with the EMA and FEM results. As described by Peeters and De Roeck [20], the time-domain methodologies estimate the modal model based on a state-space representation of the system obtained from the time-domain data, while the frequency-domain approaches identify the modal parameters from power spectral density functions of output responses, see [21], [22]. Very often, the real-life structures to be monitored are exposed to nonstationary and even severe ambient excitation. Within such context, it is therefore of paramount importance to study the influence of the system non-linearity on the output-only modal estimation for the structural damage detection. There are several techniques for the application of the OMA method, including Frequency-Domain Decomposition (FDD), Hilbert Transform Method (HTM), Stochastic Subspace Identification (SSI), Transmissibility Based Operational Modal Analysis (TOMA), Blind Source Separation technique (BSS). In this work, the FDD technique was used to derive the vibrating modes of the structure. For a complete theoretical background, see [17], [23].

Another important study is the taxi vibration test, which can be performed either as an alternative to the GVT or as a supplement to conventional ground testing, see [12], [24]. In contrast to a conventional GVT, which employs artificial excitation, natural excitation is used in taxi vibration testing. The TVT described in this work make use of output-only vibration measurements acquired while the aircraft is driving on the uneven taxiway. Therefore, it can provide modal parameters of the aircraft for Finite Element (FE) model validation to achieve permission for the first flight test. Göge [25] described an automatic updating of large aircraft models using experimental data from ground vibration testing. Thomas *et al.* [26] presented a new high fidelity reduced order modeling based on a hybrid stick model for aircraft dynamic aeroelasticity analysis. TVT can be combined with in-flight tests to achieve a significant reduction in time.

Once the modes were acquired, a flutter clearance using modal test data and NASTRAN [27] DMAP alters was performed in the last part of the paper both for the isolated wing and full-aircraft. The method utilized here was inspired by the study of Byun and Jun [28], who performed a preliminary flutter analysis utilizing modal test data. Another method for performing a flutter prediction is described by Zhang *et al.* [29]. Nicolosi *et al.* [30] performed flight simulations and flight tests to evaluate roll performance assessment of a light aircraft.

This article is organized as follows: (i) Section 2 introduces the experimental set-up for the different static and dynamic tests; (ii) the analysis and the results obtained both from static and dynamic tests are shown in Section 3, along with a validation against a finite element model; (iii) finally, in Section 4, the main conclusions are discussed.

2 Experimental set-up and procedures

For illustrative purposes, Fig. 1 shows the Dardo Aspect aircraft at the Aeroclub of Turin, Italy. Dardo is a wet-laminate full-composite aircraft designed by C.F.M. Air for low-cost, high-efficiency military screening and initial training. The maximum take-off weight is W= 700 kg, the wing-span is b= 8.4 m, and the aircraft length is L= 7 m.

2.1 Static tests

The first part of the investigation deals with the static tests. Figure 2 shows the wing attached to the ad-hoc test rig used to simulate the wing connection to the fuselage. The load was applied through a hydraulic piston. The wing-up bending test was realized by distributing the piston load

Figure 1: CFM Air Dardo Aspect.

at the location of the ribs. Full-field displacements and strain acquisitions were done by using DIC,

Figure 2: Experimental set-up of the wing used for the static response analysis.

although this technique is not yet usable for certification. In DIC, in fact, calibration (Fig. 3) is not unique, but it is very important because the accuracy of the acquisition is affected by the image parameters and by the quality of the random surface pattern, which is necessary to draw on the surface of interest. In fact, it is recommended to create a superficial pattern with a smooth transition from black and white. For a complete description of these procedures and the instrumentation used in this analysis, see [6].

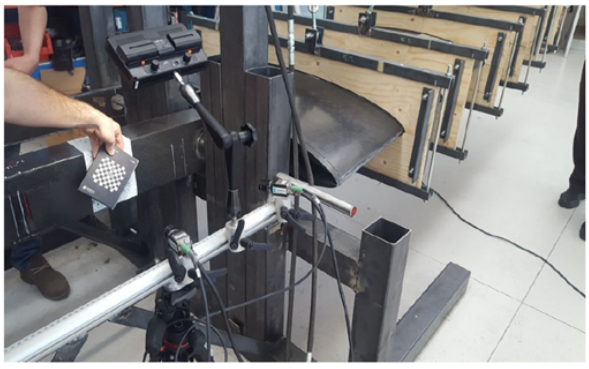

Figure 3: Experimental set-up of the wing used for the static response analysis.

2.2 Dynamic tests

Figure 4 shows the arrangement of the isolated wing. The same wing was used for ultimate load wing-up bending test. In the GVT analysis, the entire loading structure (test rig) was detached (Fig. 4a) and the wing was anchored to the rigid structure by using elastic cables, see Fig. 4b. In this manner, nonlinearities are intended to be isolated, and free boundary conditions are simulated. Accelerometers were opportunely located based on the numerical simulations, with the aim

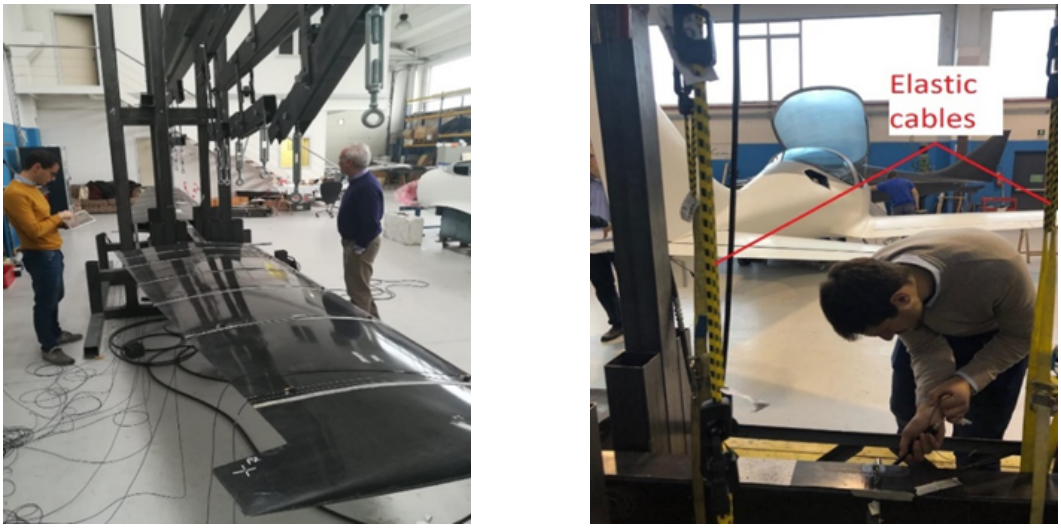

(a) Wing attached to the test rig (b) Elastic cables to simulate free condition

Figure 4: GVT arrangement of the Dardo wing.

of measuring all the important natural frequencies and mode shapes. The exact positions of the accelerometers of the wing are shown in Fig. 5. The experimental modal analysis [31] was per-

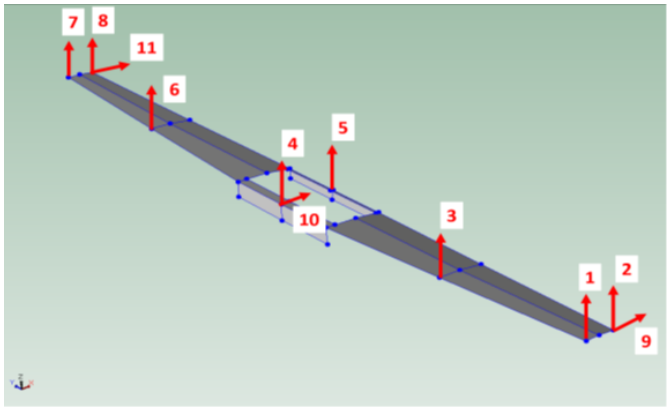

Figure 5: Reference points in the in-plane and out-of-plane directions. Wing under free boundary conditions.

formed by exciting the structure through an impact hammer and using twelve accelerometers. All the analyses and experiments are carried made with a real-time, multichannel sound and vibration

data acquisition hardware by Brüel & Kjaer. This latter is made of 12-ch. Input Module LAN-XI 25.6 kHz Type 3053, and a rechargeable Lithium-Ion battery module. The response of the structure due to the excitation is measured with a maximum of 12 accelerometers from DeltaTron and having a sensitivity of 10 mV/ms2. The accelerometers are uni-axial. Excitation is provided by using an impact hammer Type 8206 from Brüel & Kjaer with medium-soft to hard head tips. Although there are 12 channels available, 11 are used for acquisition, and the last is connected to the hammer, which means that the location of the accelerometers is fixed during the analysis and the hammer rovers. For each point, a total of 10 measurements are carried out. All the tests were performed in a frequency range of 0-100 Hz.

Figure 6a shows the experimental set-up for the analysis of the full-aircraft. There are several suspension methods [2], which are used during the GVT of an airplane or its components, depending on the size and weight of the structure. Generally, preferred methods make use of suspension bungee cords or dedicated springs. Interested readers are referred to Whitney *et al.* [32], who provided a detailed discussion of suspension methods. For this configuration, the aircraft with retracted landing gear was suspended with two dedicated springs to simulate free-free boundary condition and minimize leak and non-linear effects. The single spring, shown in Fig. 6b, has the following characteristics: rest length, L_0= 92 cm; maximum elongation under a mass of 220 kg, Lmax= 58 cm; fundamental frequency of the spring-mass system (Dardo empty mass= 450 kg), f= 0.65 Hz; stiffness, k= 3721 N/m. For this measurements, the twelve accelerometers were located near the

(a) Suspended aircraft

(b) Representation of the spring

Figure 6: GVT arrangement of the full-aircraft.

inspection drawers, and with the aim of measuring all the important frequencies and mode shapes. The exact placements of the accelerometers are shown in Fig. 7. The main purpose of these tests was to characterize the dynamic behavior of the aircraft, but also to make an EMA-OMA correlation rather than the validation of a finite element model against the experiments.

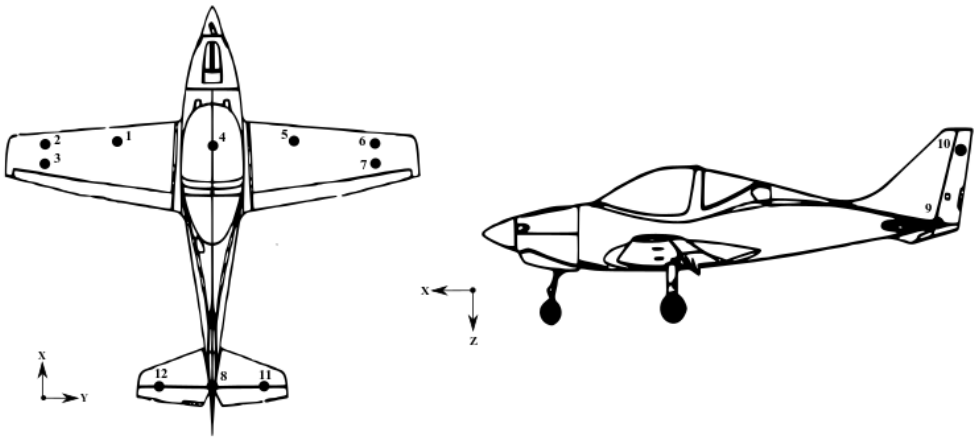

Figure 7: Reference points on the top (acc. direction along Z) and side (acc. direction along Y) views of the full aircraft.

2.3 Flutter clearance

The preliminary evaluation of flutter was performed by coupling calculated GVT modes to analytical panel methods (DLM) by Nastran and dedicated DMAP alter. Figure 8 presents a chart diagram illustrating the computation procedure of flutter analysis with GVT modal data. As a preliminary investigation, the effects of control surfaces were not considered, and only the modes of the primary structures were analyzed. Finally, flight tests were performed to study operational modal analysis using different sources of excitation. In particular, typical flight conditions were analyzed.

3 Results discussion

3.1 Full-field DIC measures

The measurements of true full-field displacements and strains were performed in correspondence of the web of the main spar. This area is the one highlighted in red in Fig. 9, and shown in Fig. 10 during the DIC acquisition. DIC was used in the range 0 – 240 % of the limit load, as shown in Table 1 and, for higher loads (240-300%), it was removed for safety reasons. Figure 11 shows the results both of the vertical displacements and the axial strains as a function of the applied load. By increasing the applied load, the vertical displacements remain fairly linear, so the strains. This

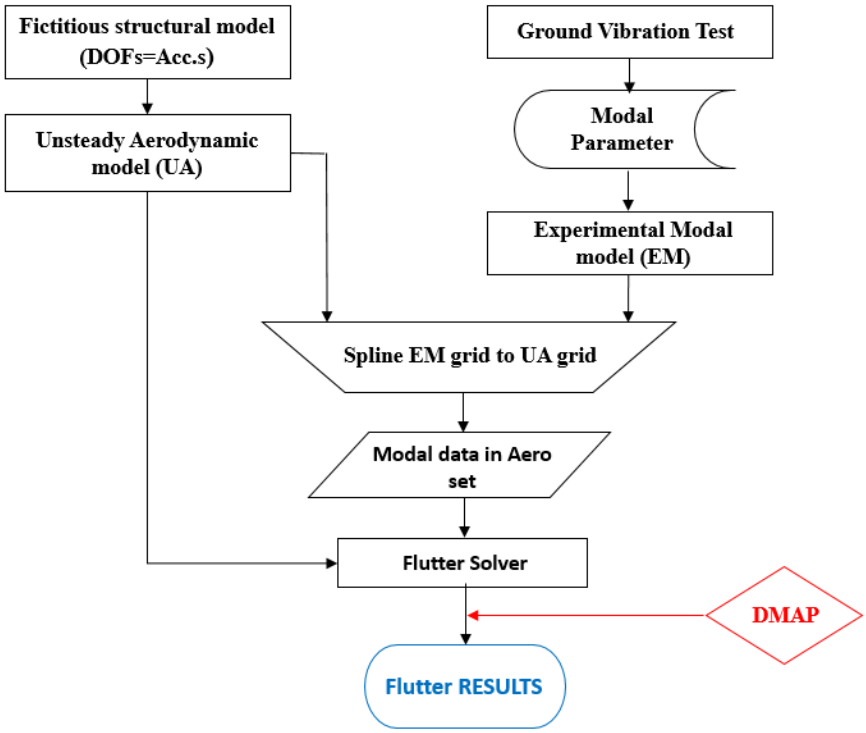

Figure 8: Schematic diagram for flutter analysis using test modal data.

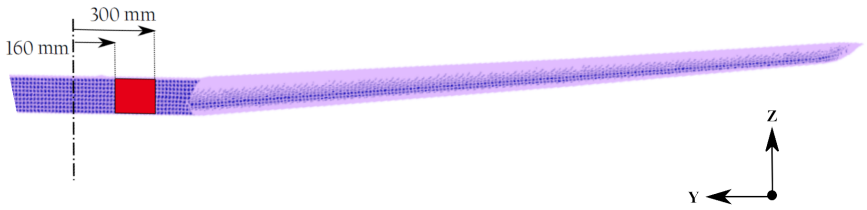

Figure 9: Front view of the composite wing. Test area in red. Spar web at the wing root.

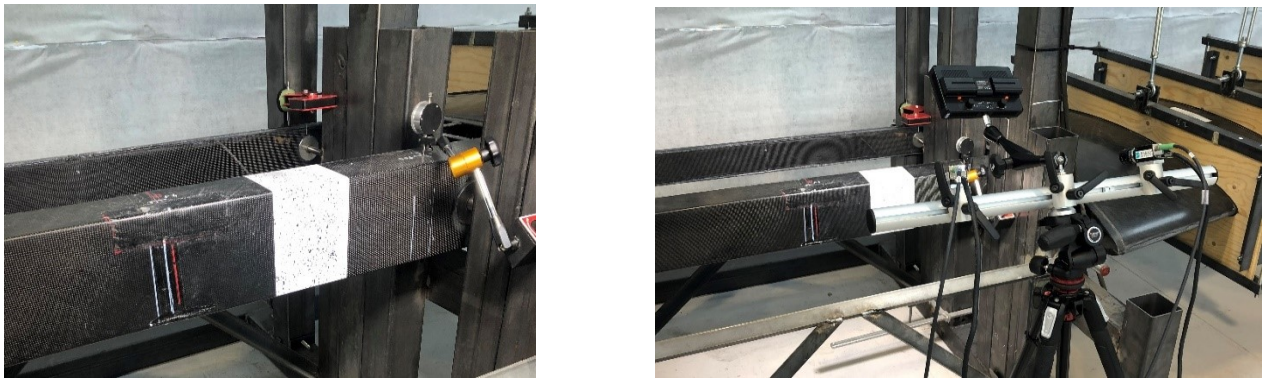

Figure 10: Test area after superficial treatment and during image acquisition.

	Load [kgf]	Load [% limit load]
0	0	-
1	154	0
2	628	50
3	1040	100
4	1560	150
5	1608	160
6	1700	170
7	1800	185
8	1855	190
9	1938	200
10	2075	210
11	2126	225
12	2165	225
13	2234	230
14	2393	240

Table 1: Applied load during the test.

demonstrated the high stiffness of the wing. Furthermore, the graph of the deformations shows, in particular near 200% of the limit load, some local failures, accompanied by hearable the noise during the test; these were some structural failures due to the fibers rupture. Figure 12, instead, depicts the variation of the strain (ϵ_{xx}) with respect to the web thickness (y). As expected, the neutral axis passes through the zero and maintains a linear trend for the various load steps. Figure 13

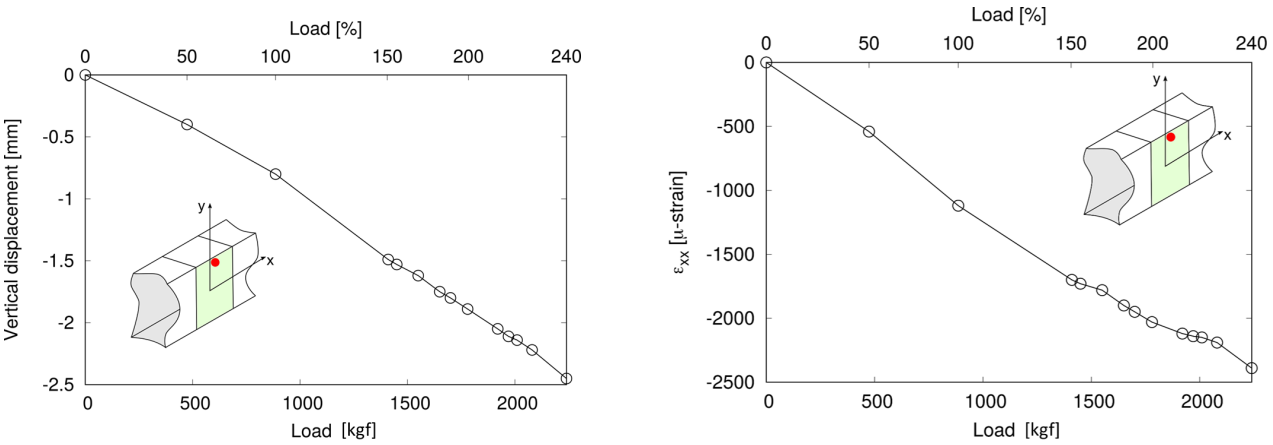

Figure 11: Vertical displacements and axial strain versus applied load.

shows some numerical results of the axial strain at 100% and 240% of the limit load. Furthermore, in Fig. 14 and 15, a comparison with a finite element model is reported [6]. The main objective was to validate failure predictions based on the FE model. These results show a good correspondence between DIC and FEM data.

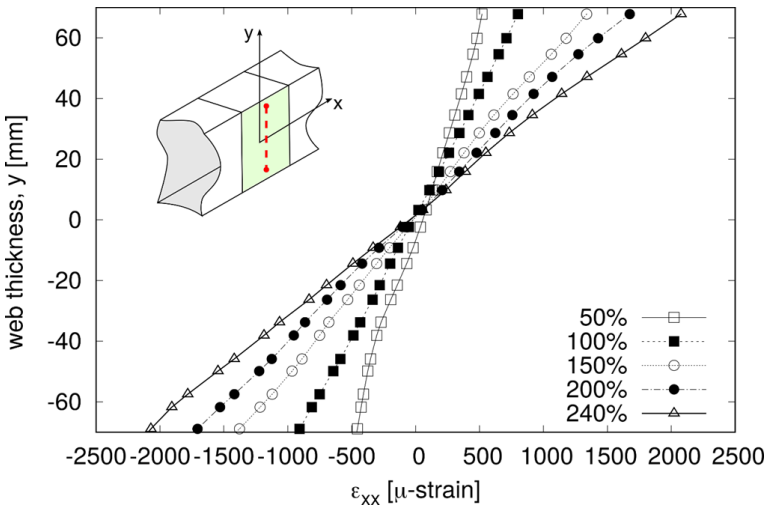

Figure 12: Web thickness versus axial strain.

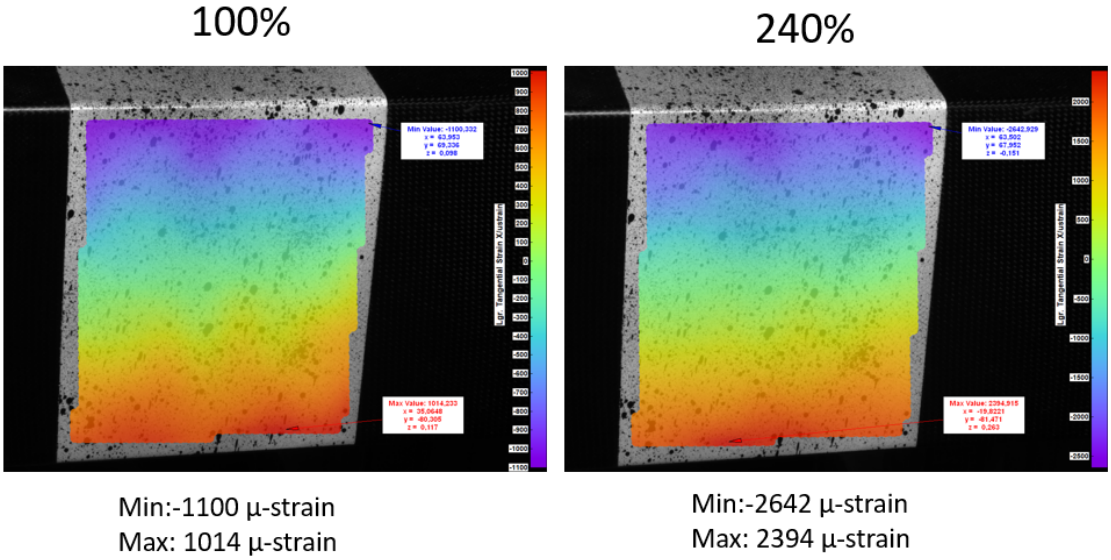

Figure 13: 3D map of the axial strain for 100% and 240% limit loadings.

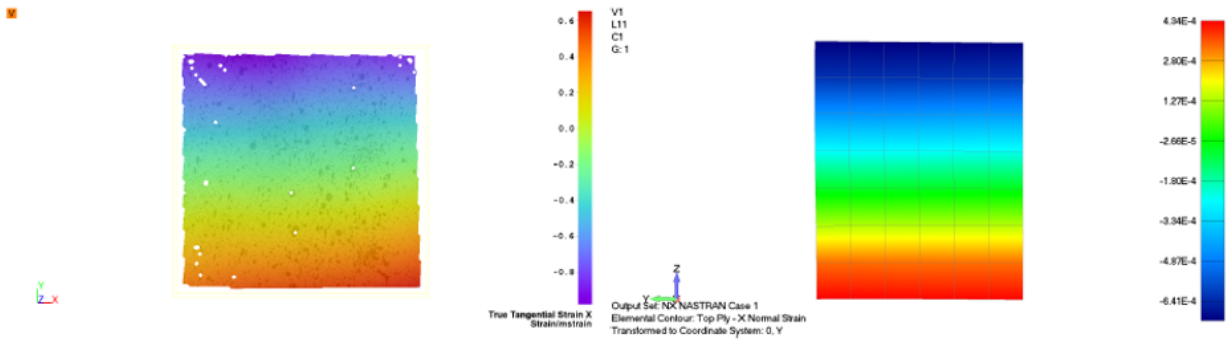

Figure 14: Comparison between DIC and FEM. True strain ϵ_{xx} on test area. Note that DIC results are given as microstrains.

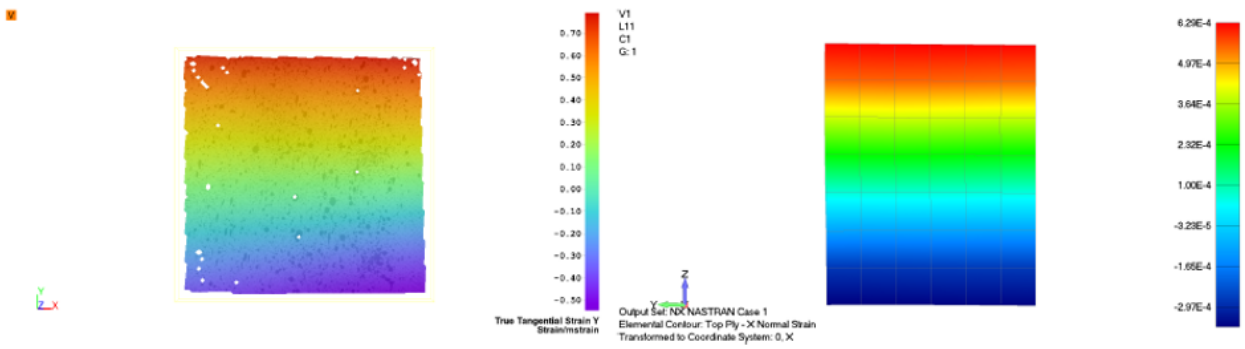

Figure 15: Comparison between DIC and FEM. True strain ϵ_{yy} on test area. Note that DIC results are given as microstrains.

3.2 Natural frequencies and mode shapes

First, ground vibration tests of the isolated wing and the full-aircraft are carried out using both OMA and EMA method. A preliminary flutter clearance is conducted to get some useful information for the subsequent flight tests. Next, a taxing vibration test is performed to show its reliability in comparison with GVT results. Finally, some flight test results obtained adopting the OMA procedure are shown.

3.2.1 Ground vibration test

In the case of the wing, modal parameters were carried out by the EMA method, and a comparison with the FEM results is reported. Once the measurements were acquired through a hammer test, the EMA method provides the various FRFs where it is possible to observe the presence of modal peaks. Figure 16 shows an example of the accelerometer acceleration signal and phase-magnitude graph obtained. As far as the quality of the measurements is concerned, one may observe another important parameter that is the coherence function. In EMA, cross-spectrum vs input signal are used to identify the natural frequencies, damping, and mode shapes. As reported by Rahman *et al.* [33], the transfer function (H_1) can be derived from dividing the auto power spectrum of output by the cross power spectrum of the input and output. Similarly, the transfer function (H_2) can be derived by dividing the cross power spectrum of the input and output by the auto power spectrum of the input. The coherence function, γ^2, is the ratio of H_2 and H_1. The coherence function is used as a data quality assessment tool which identifies how much of the output signal is related to the measured input signal. It can be shown that γ^2 lies between 0 and 1. Coherence near 1 indicates that both $H_1(\omega)$ and $H_2(\omega)$ are in very close agreement, which implies that the measurements are believable and that noise and non-linear effect are not significant. In Fig. 17, an example of a

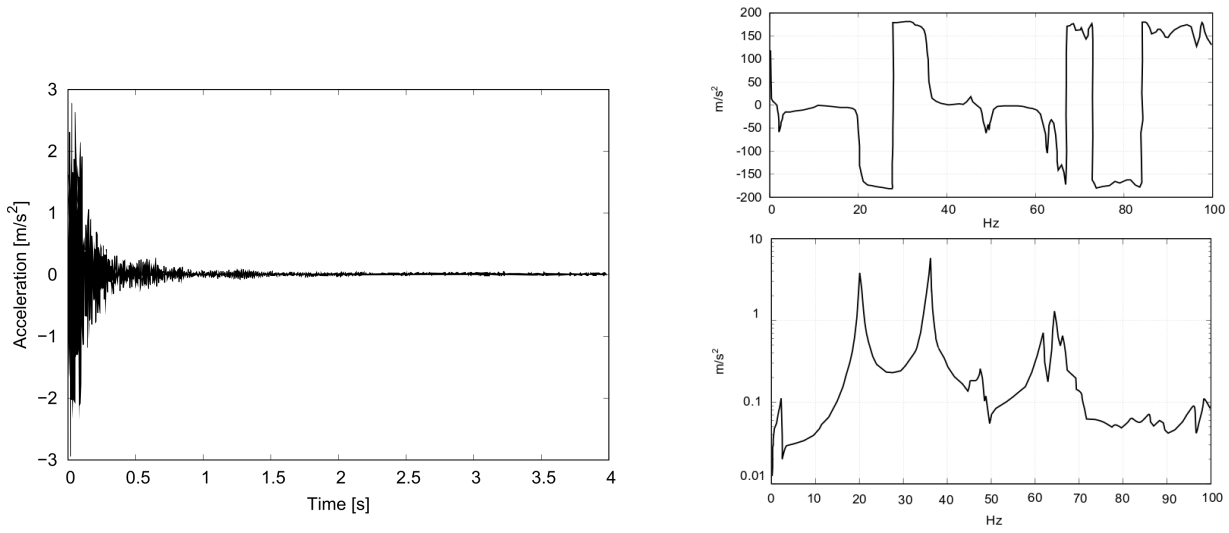

(a) Acceleration signal

(b) Phase-Magnitude, H_{xy}

Figure 16: Measured data ref. point 1, see Fig. 5.

coherence function obtained is reported. In Table 2, the results for the first five elastic modes are shown. In Figs. 18 to 22 the representation of the most important mode shapes of the structure

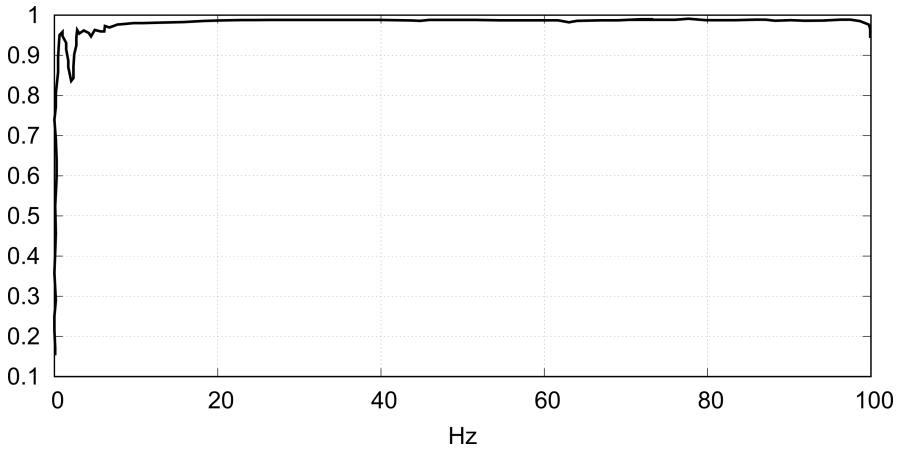

Figure 17: Coherence function, γ^2_{xy}.

are given. EMA results show a good correspondence with FEM. An orthogonality check among EMA modes is carried out in Fig. 23. It is shown that there is a minor discrepancy between modes 2 and 3, demonstrating the slight frequency differences in Table 2. In fact, MAC is a scalar indicating correspondence between two sets of mode shapes, see [34, 35].

In the case of the full-aircraft (see Fig. 6a), a comparison between EMA and OMA methods is shown. In the case of OMA, (not-measured) random loadings were applied to the suspended aircraft. In Table 3, the results acquired by GVT analysis are summarized. In Fig. 24, important mode shapes of the aircraft structure are shown. For the sake of completeness, an orthogonality check using MAC

Mode #	EMA [Hz]	FEM [Hz]	Description
1	20.08	22.34	First symmetric wing bending
2	32.42	36.41	First anti-symmetric wing torsion
3	35.73	43.53	Anti-symmetric bending - Anti-symmetric torsion
4	48.14	53.14	Edgewise bending
5	64.46	65.01	Second symmetric wing bending

Table 2: Comparison between EMA and FEM results, suspended wing.

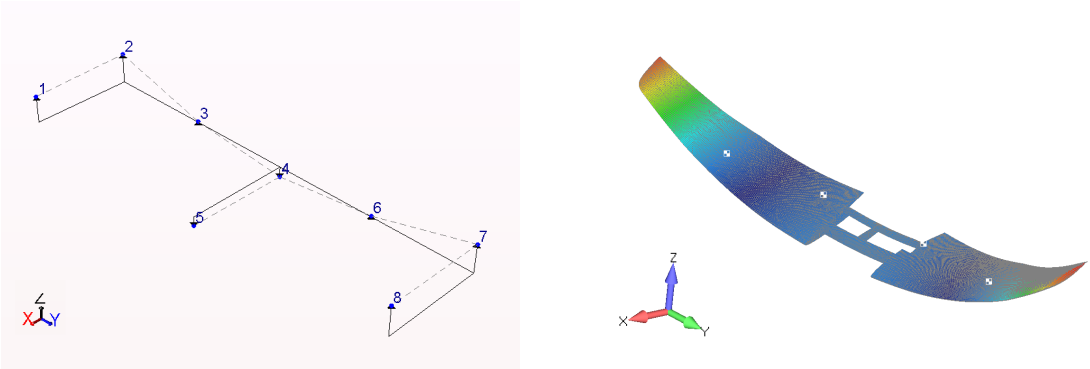

(a) EMA (b) FEM

Figure 18: Mode 1.

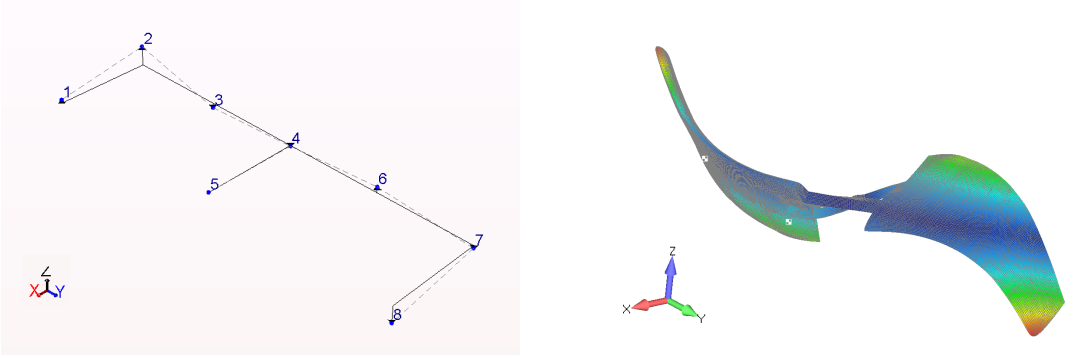

(a) EMA (b) FEM

Figure 19: Mode 2.

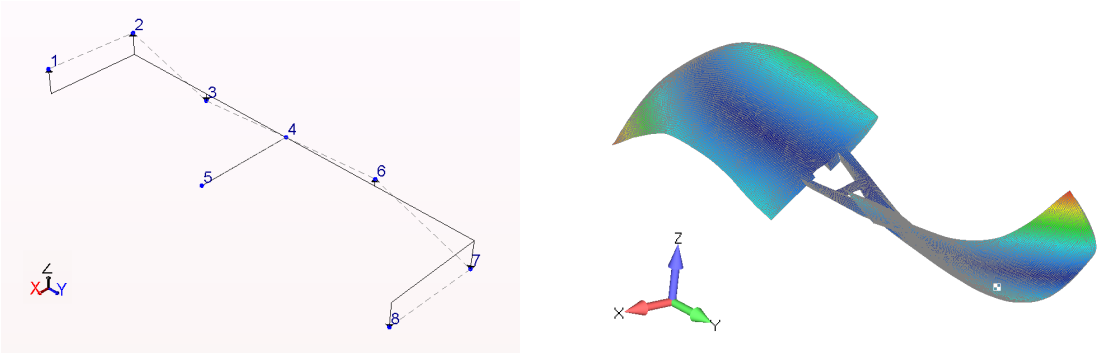

(a) EMA (b) FEM

Figure 20: Mode 3.

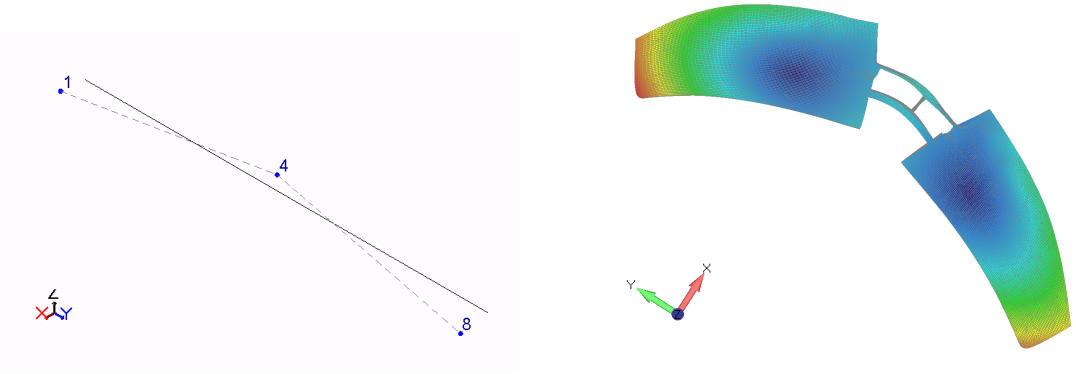

(a) EMA (b) FEM

Figure 21: Mode 4.

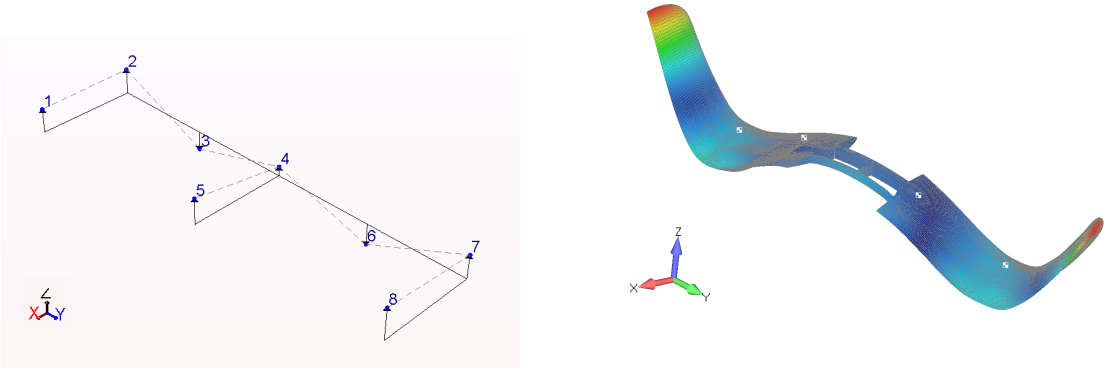

(a) EMA (b) FEM

Figure 22: Mode 5.

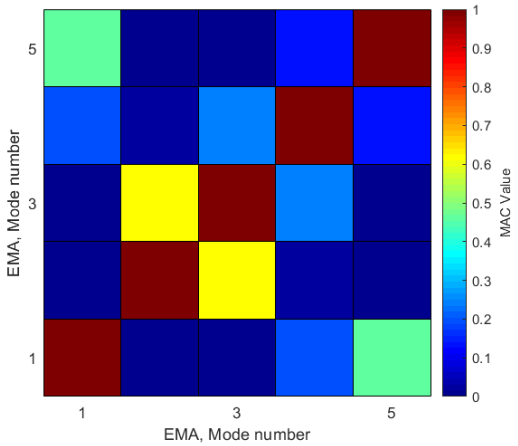

Figure 23: Orthogonality check using MAC, suspended wing.

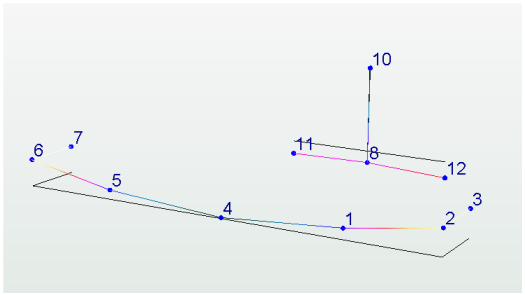

(a) Mode 1

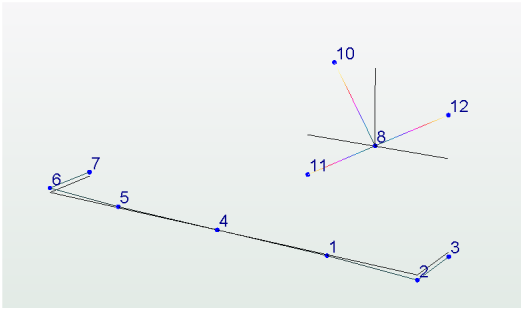

(b) Mode 2

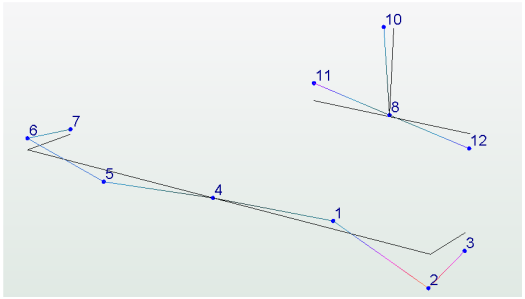

(c) Mode 3

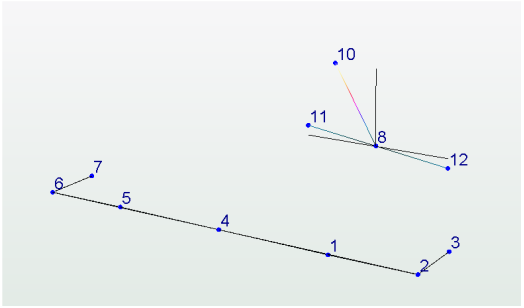

(d) Mode 4

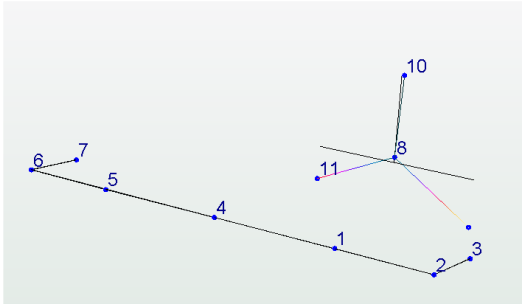

(e) Mode 5

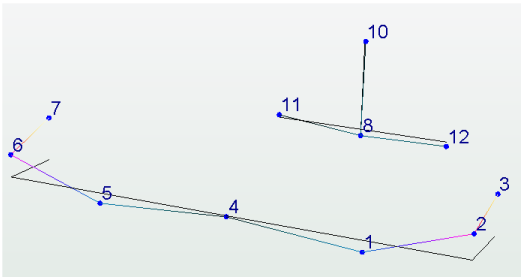

(f) Mode 6

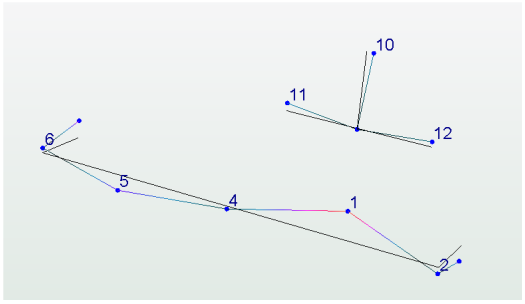

(g) Mode 7

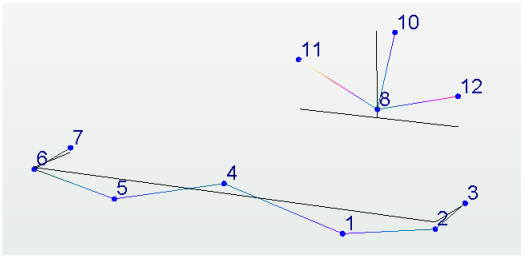

(h) Mode 8

Figure 24: Mode shapes of the entire aircraft.

Mode #	EMA [Hz]	OMA [Hz]	Description
1	11.142	10.986	First wing symmetric bending & fuselage bending
2	14.499	14.450	First wing anti-symmetric bending & H-tail anti-symmetric bending
3	22.437	21.240	Second wing anti-symmetric bending + torsion & H-tail anti-symmetric bending & first fin bending
4	25.307	26.855	Second fin bending
5	36.317	36.148	First H-tail symmetric bending
6	41.451	43.500	Second wing symmetric bending & torsion
7	47.833	49.000	Second wing anti-symmetric bending & anti-symmetric torsion
8	49.935	50.500	Third wing symmetric bending & H-tail symmetric bending

Table 3: Comparison between EMA and OMA results, suspended aircraft.

is illustrated in Fig. 25. The results obtained confirmed the OMA methodology, which is reliable

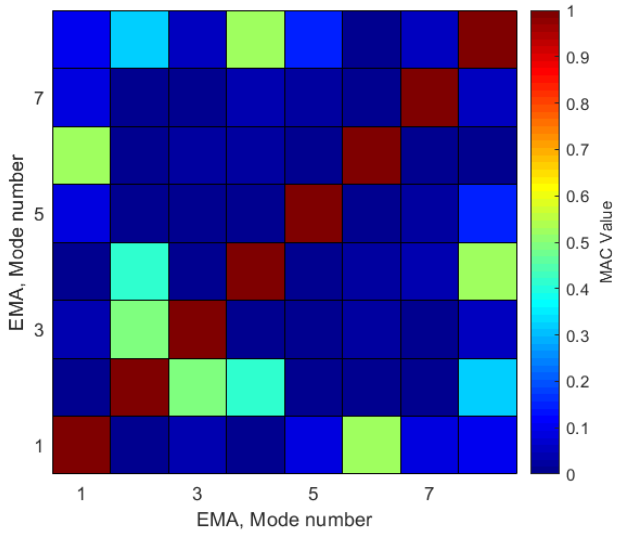

Figure 25: Orthogonality check using MAC, full-aircraft.

for the problem under consideration and applicable to subsequent flight tests, when input loadings will not be measured.

3.2.2 Flutter clearance

Once the modes were acquired, a preliminary flutter clearance was performed both for the isolated wing and full-aircraft. As already mentioned, this flutter analysis was carried out considering fixed commands. The evaluation of the flutter was performed by couplings calculated GVT EMA modes to analytical panel methods by Nastran and dedicated DMAP alter. In Figs. 26 and 27, the case of the isolated wing is shown. In Fig. 28-29, the results for the full-aircraft are shown. From these preliminary results and under the hypotheses done, it is reasonably clear that the aircraft does not

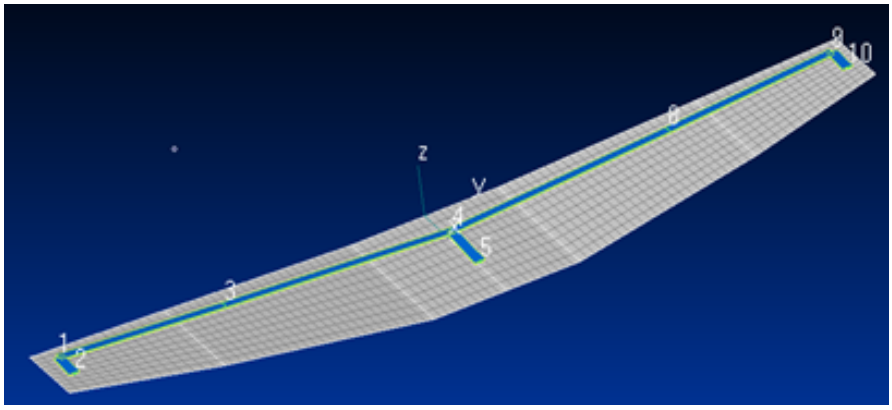

Figure 26: GVT modes coupled with Nastran aerodynamic model. Wing.

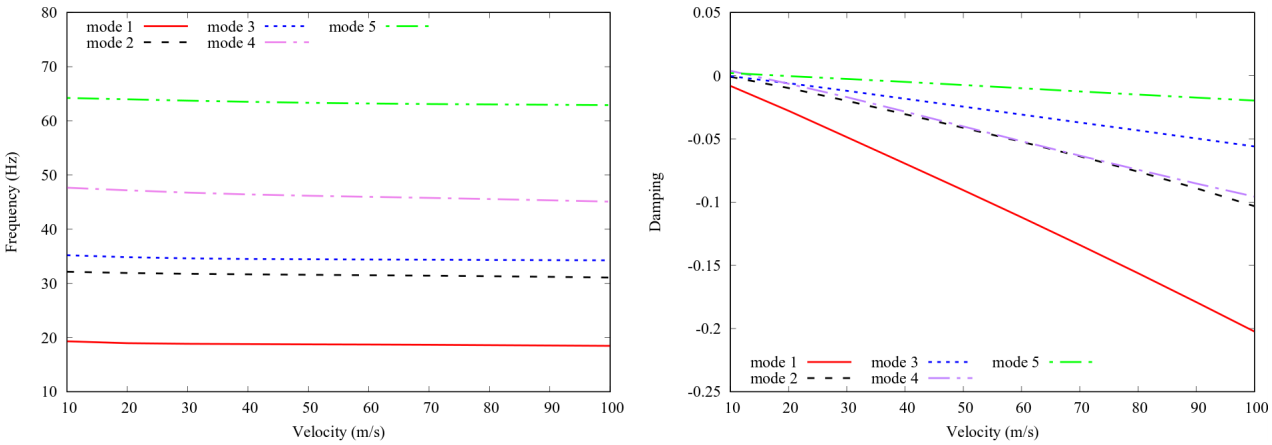

Figure 27: Frequency and damping versus velocity for the isolated wing.

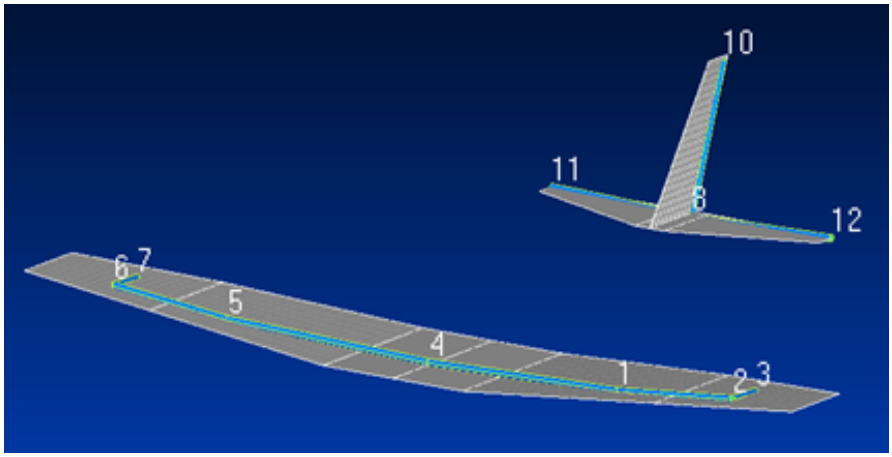

Figure 28: GVT modes coupled with Nastran aerodynamic model. Full-aircraft.

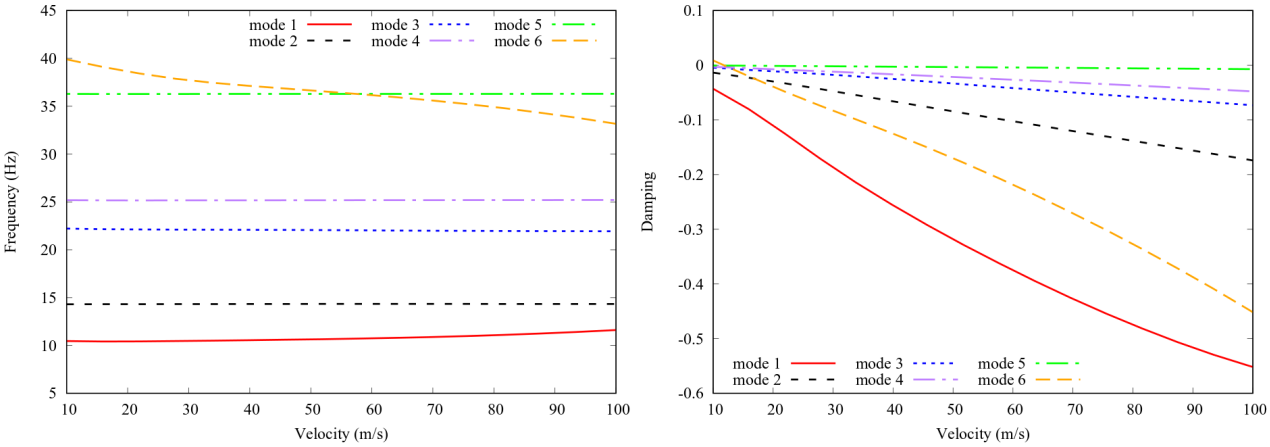

Figure 29: Frequency and damping versus velocity for the full-aircraft.

suffer any flutter phenomena. It is interesting although the mode crossing between modes 5 and 6 at about 50 m/s.

3.2.3 Taxing vibration test

As mentioned above, TVT can be an alternative to the GVT with time and cost reduction or to provide additional information. OMA was applied to obtain the natural frequency and relative mode shapes of the structure in this case. Figure 30 depicts the aircraft during TVT at the Aeroclub of Turin. In Table 4 the results obtained using the TVT confirmed GVT OMA data, and therefore the applicability of this test for this type of evaluation.

Figure 30: OMA acquisition during taxing vibration test.

3.2.4 Flight test

Finally, the results of a flight test using the OMA method are briefly discussed. Here, the timeline of the flight is divided into five regions, and the flight map is reported in Fig. 31. In Table 5, instead, the variation of the frequencies for mode 1 and 6 by varying the velocity in comparison with the FEM results are shown. As clear from Fig. 32, there is a good correspondence between experimental data

Mode #	OMA TVT [Hz]	OMA GVT [Hz]
1	10.986	10.986
2	14.343	14.450
3	21.057	21.240
4	26.550	26.855
5	35.400	36.148
6	42.894	43.500
7	48.218	49.000
8	49.733	50.500

Table 4: Comparison between TVT and GVT.

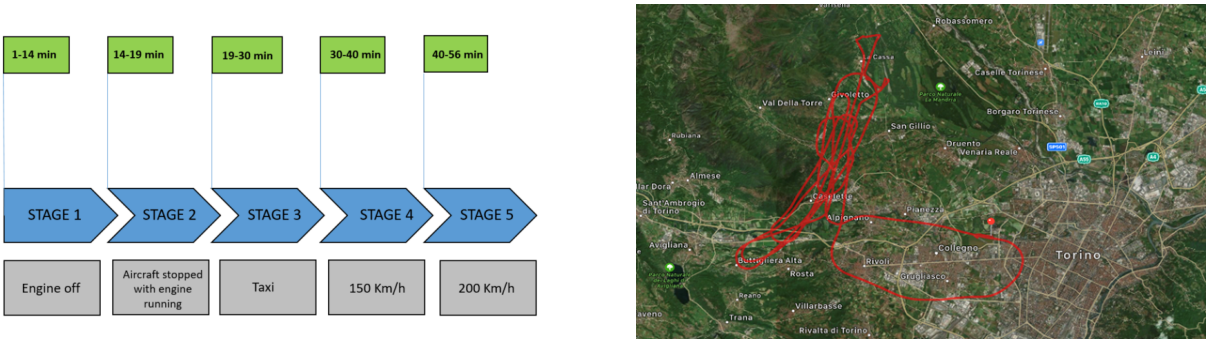

Figure 31: Timeline of the flight and the flight map.

and FEM results. Furthermore, Fig. 33 shows a comparison between the damping acquired through the OMA method using the EFDD technique [36], and the damping obtained from the half-power bandwidth of the normalized response.

4 Concluding remarks

This work has discussed some important results from the testing campaign of the Dardo Aspect, a full-composite VLA. As far as static tests are concerned, results from the Digital Image Correlation technique have been documented in terms of both displacements and in-plane strains. Comparisons with a FE model have been provided, and they demonstrate good agreement between test and numerical results. The resulting accuracy, reliability, and practicability of the DIC application

Velocity $[km/h]$	Bending (I) OMA $[Hz]$	Bending (I) FEM $[Hz]$	Torsion (VI) OMA $[Hz]$	Torsion (VI) FEM $[Hz]$
10	11.19	10.46	39.50	39.98
150	11.44	10.56	37.07	37.13
200	11.69	10.68	35.85	36.35

Table 5: Variation of the 1^{st} and 6^{st} mode frequencies with respect to flight velocities.

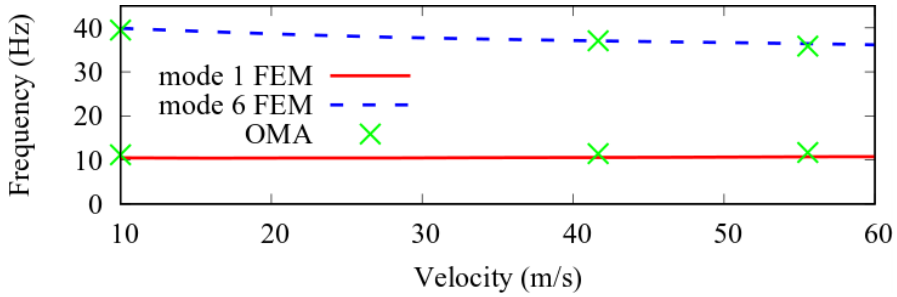

Figure 32: Variation of natural frequencies vs flight speed from FE model and flight tests.

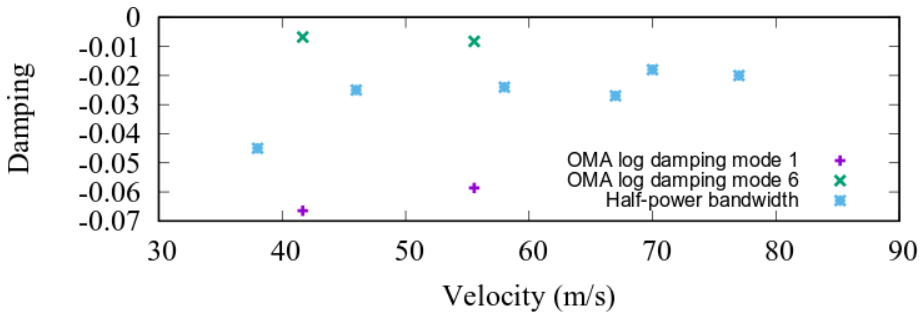

Figure 33: Comparison of the damping obtained by OMA method with that obtained from the half-power bandwidth of the normalized response.

for aerospace structures confirm this technology as an enabling practice for continuous full-field displacement and strain measurements. Currently, no standards exist to assess the metrological performances of DIC. Clearly, it is desirable that such procedures emerge so that DIC measurements become acceptable to certification agencies. Nevertheless, not all strain measurement scenarios are appropriate for DIC; e.g. high frequency or low strain measurements. Furthermore, it is still generally preferred to use conventional devices for simple displacement measurements in a single direction.

Regarding the dynamic tests, the OMA method turned out to be an excellent alternative to the classical EMA to determine the modal properties of the structures with a significant reduction in testing time. Moreover, TVT, showing a good agreement with the GVT data, presents an excellent choice for this type of analysis. Nevertheless, when compared to classical flight vibration testing techniques, OMA is more sensitive to measurement chain noise and sensors quantity. Future research should address this aspect.

Acknowledgments

This research has been co-funded by Embraer S.A.

References

[1] M. Walz. The dream of composites. *R&D MAGAZINE*, 48(11):34–36, 2006.

[2] W. Szkudlarek, A. Mizutani, B. Peeters, M. Luczak, and M. Kahsin. Ground vibration testing, finite element modeling and correlation of a composite hobby aircraft. In *13th International Conference on Aerospace Sciences and Aviation Technology, Cairo, Egypt*, 2009.

[3] H. Yan, Z. Qin, W. Zhang, A. Ming, X. Wang, and F. Chu. Dynamic analysis of laser shock response: Experimental and numerical studies. *Aerospace Science and Technology*, 94:105430, 2019.

[4] A. Pagani, M. Petrolo, G. Colonna, and E. Carrera. Dynamic response of aerospace structures by means of refined beam theories. *Aerospace Science and Technology*, 46:360–373, 2015.

[5] S.H. Daly. Digital image correlation in experimental mechanics for aerospace materials and structures. *Encyclopedia of aerospace engineering*, 2010.

[6] A. Pagani, E. Zappino, A.G. de Miguel, V. Martilla, and E. Carrera. Full field strain measurements of composite wing by digital image correlation. *Advances in aircraft and spacecraft science*, 6(1):69–86, 2019.

[7] P. Vialettes, J.M. Siguier, P. Guigue, M. Karama, S. Mistou, O. Dalverny, S. Granier, and F. Petitjean. Experimental and numerical simulation of super-pressure balloon apex section: Mechanical behavior in realistic flight conditions. *Advances in Space research*, 37(11):2082–2086, 2006.

[8] MSC Software. Md/msc nastran 2010 quick reference guide. 2010.

[9] R. Kurniawan. Numerical study of flutter of two dimensional aeroelastic system. *WCE 2013 London, U.K.*

[10] S. Hernández, E. Menga, S. Moledo, L.E. Romera, A. Baldomir, C. López, and M.C. Montoya. Optimization approach for identification of dynamic parameters of localized joints of aircraft assembled structures. *Aerospace Science and Technology*, 69:538–549, 2017.

[11] B. Peeters, W. Hendricx, J. Debille, and H. Climent. Modern solutions for ground vibration testing of large aircraft. *Sound and vibration*, 43(1):8, 2009.

[12] M. Böswald, J. Schwochow, G. Jelicic, and Y. Govers. New concepts for ground and flight vibration testing of aircraft based on output-only modal analysis. In *7th International Operational Modal Analysis Conference*, 2017.

[13] D.F. Voracek. Ground vibration and flight flutter tests of the single-seat f-16xl aircraft with a modified wing. 1993.

[14] M.W. Kehoe and L.C. Freudinger. Aircraft ground vibration testing at the nasa dryden flight research facility, 1993. 1994.

[15] G. Gloth, M. Degener, U. Füllekrug, J. Gschwilm, M. Sinapius, P. Fargette, B. Levadoux, and P. Lubrina. Experimental investigation of new gvt concepts for large aircraft. *Sound and Vibration*, 35(11):14–18, 2001.

[16] J. Simsiriwong and R.W. Sullivan. Vibration testing of a carbon composite fuselage. *Low Frequency Noise & Vibration*, 30(2):166, 2011.

[17] N. Ameri, C. Grappasonni, G. Coppotelli, and D.J. Ewins. Ground vibration tests of a helicopter structure using oma techniques. *Mechanical Systems and Signal Processing*, 35(1-2):35–51, 2013.

[18] T. De Troyer, P. Guillaume, C. Devriendt, and M. Runacres. Combined use of frfs and transmissbility functions in an omaxframework. In *Proceedings of ISMA2010–International Conference on Noise and Vibration Engineering including USD2010*, pages 3263–3273, 2010.

[19] E. Neu, F. Janser, A.A. Khatibi, C. Braun, and A.C. Orifici. Operational modal analysis of a wing excited by transonic flow. *Aerospace Science and Technology*, 49:73–79, 2016.

[20] B. Peeters and G. De Roeck. Reference-based stochastic subspace identification for output-only modal analysis. *Mechanical systems and signal processing*, 13(6):855–878, 1999.

[21] R. Brincker, L. Zhang, and P. Andersen. Modal identification from ambient responses using frequency domain decomposition. In *Proc. of the 18*'International Modal Analysis Conference (IMAC), San Antonio, Texas*, 2000.

[22] R. Brincker. Some elements of operational modal analysis. *Shock and Vibration*, 2014, 2014.

[23] E. Zhang, R. Pintelon, and P. Guillaume. Modal identification using oma techniques: nonlinearity effect. *Shock and Vibration*, 2015, 2015.

[24] M. Boswald and Y. Govers. Taxi vibration testing-an alternative method to ground vibration testing of large aircraft. In *International Conference on Noise and Vibration Engineering (ISMA2008)*, 2008.

[25] D. Göge. Automatic updating of large aircraft models using experimental data from ground vibration testing. *Aerospace science and technology*, 7(1):33–45, 2003.

[26] P.V. Thomas, M.S.A. ElSayed, and D. Walch. Development of high fidelity reduced order hybrid stick model for aircraft dynamic aeroelasticity analysis. *Aerospace Science and Technology*, 87:404–416, 2019.

[27] MSC Nastran. Aeroelastic analysis user's guide. *CA, USA, Version*, 68, 2004.

[28] K.H. Byun and S.M. Jun. Flutter analysis of f-16 aircraft utilizing test modal data. *ICAS2006*, 2006.

[29] W. Zhang, Z. Lv, Q. Diwu, and H. Zhong. A flutter prediction method with low cost and low risk from test data. *Aerospace Science and Technology*, 86:542–557, 2019.

[30] F. Nicolosi, A. De Marco, V. Sabetta, and P. Della Vecchia. Roll performance assessment of a light aircraft: Flight simulations and flight tests. *Aerospace Science and Technology*, 76:471–483, 2018.

[31] P. Avitabile. Experimental modal analysis. *Sound and vibration*, 35(1):20–31, 2001.

[32] M.J. Whitney, J.L. Panza, and R.D. Brillhart. Gvt suspension effects on correlation of the predator b vehicle. In *SPIE proceedings series*. Society of Photo-Optical Instrumentation Engineers, 2002.

[33] A.G.A. Rahman, Z.C. Ong, and Z. Ismail. Enhancement of coherence functions using time signals in modal analysis. *Measurement*, 44(10):2112–2123, 2011.

[34] R.J. Allemang. The Modal Assurance Criterion - twenty years of use and abuse. *Sound and Vibration*, 37(8):14–23, 2003.

[35] M. Pastor, M.and Binda and T. Harčarik. Modal Assurance Criterion. *Procedia Engineering*, 48:543–548, 2012.

[36] F. Pioldi, R. Ferrari, and E. Rizzi. Output-only modal dynamic identification of frames by a refined fdd algorithm at seismic input and high damping. *Mechanical Systems and Signal Processing*, 68:265–291, 2016.